Sim-to-Real Transformer-Based Shape Reconstruction for Automated Orthopedic Fracture Reduction Planning

Sutuke Yibulayimu[1 [0000−0001−5115−9255]], Yanzhen Liu[1 [0000−0003−3766−1171]], Yudi Sang[3 (✉) [0000−0002−9971−2993]], Gang Zhu[3], Hui Li[1], Hao Lu[1], Chunpeng Zhao[2], Xinbao Wu[2], and Yu Wang[1 (✉) [0000−0003−0467−6465]]

[1] Key Laboratory of Biomechanics and Mechanobiology, Ministry of Education, Beijing Advanced Innovation Center for Biomedical Engineering, School of Biological Science and Medical Engineering, Beihang University, Beijing, 100083, China
[2] Department of Orthopaedics and Traumatology, Beijing Jishuitan Hospital, Capital Medical University, Beijing, China
[3] Beijing Rossum Robot Technology Co., Ltd., Beijing, China
{sutuk,wangyu}@buaa.edu.cn, sangyudi@rossumrobot.cn

Abstract. Accurate orthopedic fracture reduction planning is essential for ensuring successful postoperative recovery and improving patient outcomes. However, current methods are challenged by the complex and irregular fracture geometries and the scarcity of annotated training data. To address these challenges, we propose a novel approach that integrates learning-based shape restoration and fracture simulation. A transformer-based model is developed, which utilizes patch-to-patch restoration and recursive fragment registration to iteratively refine fracture reduction poses. To generate diverse and anatomically realistic fractured datasets for model training, we develop a fracture data simulation approach that combines statistical shape modeling with clinically representative fracture patterns, reducing reliance on annotated samples. Tested on extensive clinical data with hipbone and sacrum fractures, the proposed method achieved mean translational and rotational errors of 2.34 mm and 4.54°, respectively, outperforming both template-based and existing learning-based methods. Our approach enhances learning and generalization for automated fracture reduction by connecting synthetic and real-world fracture data.

Keywords: Surgery planning · Point cloud deep learning · Transformer · Fracture simulation · Statistical shape model.

1 Introduction

Fracture reduction, namely the process of realigning fractured bone fragments, is critical for optimizing biomechanical stability, promoting healing, and restoring patient mobility [14]. However, the planning process is highly subjective, time-consuming, and heavily dependent on surgeons' expertise [19]. Complex

fractures, especially in the hipbones and sacrum, further complicate the task, where even minor misalignments can lead to chronic pain and impaired functionality. These challenges highlight the need for reliable and automated reduction planning methods to determine the target pose of each bone fragment [27].

Existing automated approaches fall primarily into two categories: fracture surface matching and template-based methods. Surface matching methods align fragments based on geometric features but often fail due to the inaccuracy in segmenting and defining fracture surfaces [20,15,13,8]. Template-based methods, such as the widely used mirror-template approach [26,5,28,8], rely on predefined reference shapes. Although effective for unilateral fractures, they cannot handle bilateral fractures or bones without contralateral references, such as the sacrum. Furthermore, the alignment errors caused by anatomical asymmetries between contralateral bones should not be ignored [6].

As an alternative to the mirror template, statistical models have been studied. Early methods construct mean shapes of bones but failed to account for individual variability [4]. Statistical shape models (SSMs) capture anatomical variability and enable adaptive deformations, providing flexibility in reconstructing diverse fracture configurations [7,21,12]. However, SSM-based methods require simultaneous optimization of fragment poses and deformation parameters, often leading to suboptimal results due to local minima.

Attempts have been made to apply deep leaning in reduction planning. A PointNet-based framework has been proposed to facilitate the planning process by establishing initial correspondence between fracture fragments and templates [3]. A convolutional pose estimation network has been used to address sacroiliac joint dislocation, but has not been applied to fractures of single bones where the fracture surfaces are more complex [22,11]. A key challenge in learning-based methods is the scarcity of annotated fracture datasets. The high variability of fracture patterns calls for models with high generalizability.

Synthetic data generation offers a promising solution to data scarcity. Bidirectional frameworks have been proposed to generate fracture data and learn non-rigid transformations between healthy and fractured morphologies [25]. This method relies on real fracture data with contralateral bones for fine-tuning, introducing challenges when differences between two sides exist. Furthermore, standard convolutional networks struggle to extract meaningful features from highly variable fracture morphologies. This underscores the need for tailored feature extraction methods designed to address such variability.

In this study, we present a learning-based approach for fracture reduction planning trained with synthetic data that is only based on small datasets. Our major contributions include: (1) A transformer-based point could processing network is developed to restore intact bone shape from fractured data through fragment-aware patch encoding and patch-to-patch translation. (2) A recursive refinement strategy is implemented to iteratively improve alignment accuracy, effectively addressing diverse fracture configurations. (3) A simulation pipeline is developed, leveraging statistical shape modeling to capture anatomical variability while learning real fracture patterns.

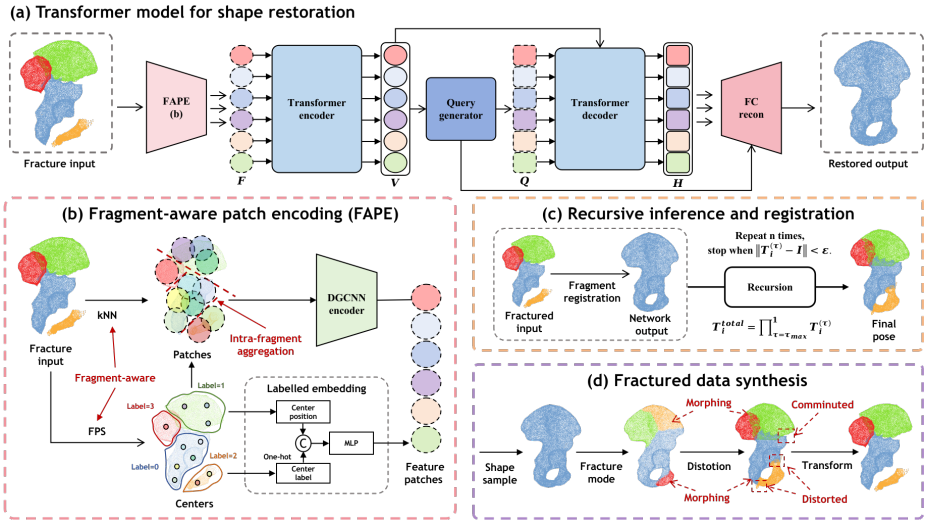

Fig. 1. Overview of the proposed method. (a) The transformer network performs patch-to-patch translation to restore bone shape. (b) FAPE encodes local features for each fragment. (c) Reduction plans are refined through recursive inference and registration. (d) Synthetic data is generated with rich variations to simulate realistic fracture.

2 Method

We aim to estimate the target pose of each fragment from surface point clouds. These point clouds are obtained by segmenting fragments in CT scans [10] and uniformly sampling points on their surfaces. As shown in Fig. 1, a transformer-based point cloud processing network is developed to restore bone shape, and a fracture data generation process is designed to support network training.

2.1 Transformer Model for Shape Restoration

Considering the variability in the number, pose, and interactions of fracture fragments, we formulate the fracture reduction planning task as a *patch-to-patch translation* problem based on transformer network, where the input is the labeled point cloud of fractured fragments, and the output is the point cloud of the reconstructed shape. A naive unified encoding for all fragments can lead to undesired interference among fragments. To mitigate this problem, we design a transformer-based network that is aware of fragment labels throughout (Fig. 1a).

Fragment-Aware Patch Encoding Fractured bones are represented by point clouds of multiple fragments. As shown in Fig. 1b, to prepare the fragments for the transformer-based model, we first sample N patch centers across all fragments. Direct application of farthest point sampling (FPS) to the entire

fractured bone may result in incomplete coverage near fragment boundaries. To address this, we allocate sampling centers proportionally to the point distribution of each fragment, and then apply FPS within each fragment to obtain center points and labels $\{s_i, \eta_i\}_{i=1}^{N}$ For each center s_i, we form a local patch P_i by selecting its k nearest neighbors (kNN) within its entire fragment.

We applied a DGCNN to encode each patch P_i through dynamic graph construction and aggregation. Compared to the original model proposed in [16], both sampling and neighborhood aggregation are performed using the fragment-aware FPS and kNN methods described above. To embed fragment-specific identity, the patch center s_i is concatenated with its one-hot encoded fragment label η_i, and then processed by a multilayer perceptron (MLP):

$$F_i = \mathrm{DGCNN}(P_i) + \mathrm{MLP}([s_i, \text{one-hot}(\eta_i)]). \tag{1}$$

After processing all N patch centers, we obtain a unified set of patch features $\mathcal{F} = \{F_1, F_2, \ldots, F_N\}$, which serves as input to the transformer modules.

Patch-to-Patch Translation with Transformers In this formulated patch-to-patch translation task, the input fractured patch features are transformed into reconstructed patch features. This process is defined as:

$$\mathcal{V} = \mathrm{ME}(\mathcal{F}), \quad \mathcal{H} = \mathrm{MD}(\mathcal{Q}, \mathcal{V}), \tag{2}$$

where ME and MD are the encoder and decoder models, $\mathcal{V} = \{V_1, V_2, \ldots, V_N\}$ are the encoded patch features, $\mathcal{Q} = \{Q_1, Q_2, \ldots, Q_N\}$ are the query embeddings, and $\mathcal{H} = \{H_1, H_2, \ldots, H_N\}$ are the reconstructed patch features. The architecture is based on the geometry-aware transformer proposed in [23].

Between the encoder and decoder, a query generator predicts query embeddings $\mathcal{Q}$ to guide reconstruction. Coarse query centers $\mathcal{C}$ are first predicted from the global feature of $\mathcal{V}$, which is extracted using max-pooling. These centers are then refined to produce the final query embeddings:

$$\mathcal{C} = \mathrm{Proj}(\mathrm{Pool}(\mathrm{Linear}(\mathcal{V}))), \quad \mathcal{Q} = \mathrm{MLP}([\mathcal{C}, \mathrm{Pool}(\mathrm{Linear}(\mathcal{V}))]), \tag{3}$$

where Proj is a linear layer that predicts 3D coordinates, and Pool is the max-pooling operation.

Coarse-to-Fine Reconstruction We adopt a multi-scale reconstruction strategy to restore bone shape. The query generator predicts local centers $\mathcal{C}$, which serve as anchors for reconstructing the point cloud. A fully connected reconstruction head f refines these centers into detailed local geometries:

$$R_i = f(H_i) + c_i, \quad i = 1, 2, \ldots, N, \tag{4}$$

where R_i represents reconstructed points around each center c_i.

The reconstruction loss is computed both at sparse level on the patch centers $\mathcal{C}$ and at dense level on the restored shape $\mathcal{R}$, using the Chamfer distance (CD) to the ground-truth point cloud $\mathcal{G}$:

$$\mathcal{L}_{\text{recon}} = \mathcal{L}_{\text{sparse}} + \mathcal{L}_{\text{dense}} = \text{CD}(\mathcal{C}, \mathcal{G}) + \text{CD}(\mathcal{R}, \mathcal{G}), \tag{5}$$

where the same dense ground truth $\mathcal{G}$ is used for both dense and sparse supervision without additional downsampling, since Chamfer Distance does not require point-wise correspondence.

Recursive Inference and Registration The restored shape serves as a template for fracture reduction. During testing, to correct errors from large initial displacements, we employ a recursive cascade approach (Fig. 1c). At each iteration τ, the network predicts a restored shape $R^{(\tau)}$, and fragments are aligned to $R^{(\tau)}$ using the iterative closest point (ICP) algorithm. This updates fragment poses and transformations $\{T_i^{(\tau+1)}\}$, which are iteratively refined until convergence ($\|T_i^{(\tau)} - I\| < \epsilon$) or a maximum iteration threshold is reached.

2.2 Training Data Simulation

To generate diverse and clinically realistic fractures for shape restoration, our method learns anatomical variations and fracture patterns from a limited set of intact and fractured samples by combining anatomical shape modeling and fracture mode labeling.

An SSM is constructed for each bone type using Point2SSM++ as the backbone network [1]. This approach establishes point correspondences across different bone geometries and applies principal component analysis (PCA) to efficiently model anatomical variability, enabling the generation of plausible bone shapes. Fracture patterns are then modeled by assigning fracture labels to the SSM based on clinical fractured data. Each SSM point is labeled according to the spatial distribution of fracture fragments observed in real samples. To ensure alignment between the SSM and fractured bones, shape deformation parameters and spatial transformations are jointly optimized [21]. This process, applied across multiple fractures, generates a diverse set of fracture modes within a unified coordinate system, forming the foundation for fracture synthesis.

Beyond the predefined fracture modes, additional variability is introduced through extensive post-processing. As illustrated in Fig. 1d, fractured samples are generated by sampling SSM shape parameters, applying a fracture mode, and incorporating morphing and distortion. The morphing step adjusts the label distribution of adjacent fracture surfaces, while distortion, which includes rotation, scaling, and shearing, alters the geometric structure to simulate irregularity in fracture surfaces commonly observed in clinical data. Further variability is introduced by randomly removing boundary regions to mimic missing shapes as in locally comminuted fracture cases. Since fragments originate from intact models without predefined interfaces, a mesh refinement algorithm [2] is employed to close open surfaces. The final fractured samples undergo randomized pose adjustments, while the intact bone serves as the ground truth for training.

3 Experiments and Results

3.1 Experimental Setup

Datasets We selected two of the most complex and challenging bone anatomies, hipbone and sacrum, to test our method. From the *CTPelvic1K* dataset [9], 430 healthy hipbone and sacrum samples were selected. They were divided into training and test sets in an 8:2 ratio for constructing the SSM. Additionally, 188 hipbone fracture cases and 52 sacrum fracture cases were selected from the *PENGWIN* dataset [10]. Due to the scarcity of fractured data, they were split in a 2:8 ratio, with 20% used for constructing the fracture modes in DFPM and 80% reserved for evaluation. In total, 191 real fracture samples were used for testing, representing one of the largest fracture test datasets to date. Ground-truth reduction poses were annotated by two clinical experts, each with more than five years of surgical planning experience.

Baseline Methods We compared the proposed network model with several fracture reduction planning methods, including average templates (Mean) [4], statistical shape templates (SSM) [21], mirrored templates (Mirror) [26], and fracture surface matching based on mirrored templates (Match) [8]. Due to their reliance on the contralateral part, mirrored-template methods were restricted to unilateral hipbone fractures only. For a fair comparison, unilateral and bilateral hipbone fracture cases were tested separately in our experiments. Additionally, a transformer-based point cloud generation method, AdaPoinTr [24], was included as a learning-based baseline.

Evaluation Reduction accuracy was assessed using translational error (in millimeter), defined as the Euclidean distance between the centers of reduced fragments and their ground truth, and rotational error (in degree), defined as the axis-angle difference between the planned and ground-truth pose matrices for each fragment. Furthermore, the reconstructed shapes were evaluated using L2 Chamfer distance (CD) (scaled by 10^{-4}) to the ground truth and part accuracy (PA) with the latter thresholded τ at 0.001 to enhance sensitivity, following established protocols [17].

Implementation The proposed network was implemented in PyTorch, with an NVIDIA RTX 3070Ti GPU. The input point clouds of fractured bones were initially downsampled to 2,048 points using FPS. Fragment labels were encoded as one-hot vectors of seven dimension. The FAPE module generated 256 patch tokens, each with 128 dimensions. And the transformer used 384 dimensions. Reconstruction was performed at the coarse level with 256 points and the fine level with 4,096 points. AdamW optimizer was used with an initial learning rate of 10^{-4} and weight decay of 5×10^{-4}, following a cosine annealing schedule. The training spanned 300 epochs with a batch size of 20. The recursive process allowed up to 10 iterations and used a convergence threshold ϵ of 1.

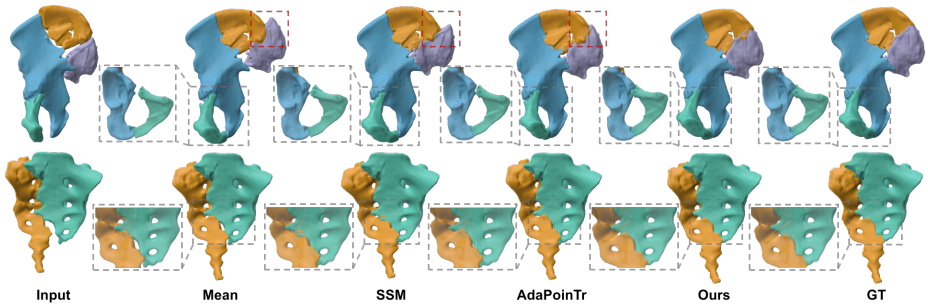

Fig. 2. Example reduction planning results for hipbone and sacrum fractures.

Table 1. Quantitative results on reduction planning for hipbone and sacrum fractures.

Method	Unilateral hipbone (76)				Bilateral hipbone (74)				Sacrum (41)			
	Rot.↓	Trans.↓	CD ↓	PA↑	Rot.↓	Trans.↓	CD ↓	PA↑	Rot.↓	Trans.↓	CD ↓	PA↑
Mean [4]	6.07	5.25	6.51	67.43	7.48	5.89	8.20	61.26	6.57	3.65	9.90	56.91
SSM [21]	5.74	4.69	5.67	74.56	6.74	5.29	7.08	62.61	6.19	3.60	9.74	60.57
Mirror [26]	5.18	3.01	3.10	89.80	–	–	–	–	–	–	–	–
Matching [8]	6.40	3.08	4.74	87.17	–	–	–	–	–	–	–	–
AdaPoinTr [24]	5.08	3.04	2.85	91.89	6.24	3.16	3.27	90.77	5.74	2.44	6.38	78.05
Our method	**4.46**	**2.35**	**2.04**	**97.04**	**4.57**	**2.51**	**1.79**	**95.72**	**4.63**	**2.04**	**4.73**	**82.11**

For data simulation, SSMs were constructed separately for the hipbone and sacrum using 344 samples, each with 38 and 11 fracture modes, respectively. Each bone had 20,000 synthesized samples, with random translation up to 15 mm and rotation up to 30° applied at each training iteration. The demonstration of data simulation is provided in the Supplementary Material. The training code and sample data are available at https://github.com/Sutuk/FracFormer.

3.2 Comparison of Reduction Planning Methods

The performance of our method was evaluated on unilateral hipbone fractures, bilateral hipbone fractures, and sacrum fractures. Results in Fig. 2 and Table 1 show that our method outperformed all baseline methods across all fracture types. Mirrored-template methods achieved competitive results due to their reliance on a contralateral healthy template, however, inherent anatomical asymmetries often led to significant remaining errors, especially in complex fracture configurations. Fracture surface matching lacks robustness due to its inability to accurately identify and align fracture surfaces. Mean templates and statistical shape templates, though applicable to all cases, struggled with individual variability and parameter optimization, leading to suboptimal performance. AdaPoinTr, which was also trained using the synthesized fracture dataset, outperformed the non-learning methods. Paired t-test indicated that the improvements provided by our method is statistical significant, with $p < 0.05$ across all metrics.

Table 2. Ablation study results. The left section evaluates different network components, while the right section examines variations in data simulation.

(a) Network Model Ablation					(b) Data Simulation Ablation				
Method	Rot.↓	Trans.↓	CD↓	PA↑	Method	Rot.↓	Trans.↓	CD↓	PA↑
w/o FAPE	5.22	2.52	2.14	95.50	w/o surface	5.34	3.20	2.93	90.33
w/o label	4.86	2.43	2.54	95.61	w/o morph.	5.17	2.56	2.06	94.89
w/o recursion	5.30	2.54	2.73	95.72	w/o distort.	5.30	2.79	2.31	95.00
Our method	**4.51**	**2.43**	**1.92**	**96.39**	Our method	**4.51**	**2.43**	**1.92**	**96.39**

Our method achieved 2.34 mm translation and 4.54° rotation errors, well within clinically accepted thresholds for fracture reduction [18].

3.3 Ablative Experiment

The contributions of the network and data simulation components were analyzed in an ablative study on the hipbone dataset. As shown in Table 2, replacing the FAPE with standard unified encoding resulted in significant performance degradation, highlighting its importance for fragment shape and pose differentiation. The incorporation of fracture label embedding expedited convergence and ensured reconstruction consistency. And removing the recursive strategy significantly reduced alignment accuracy, underscoring its role in refining fragment poses. For fractured data generation, removing key techniques such as fracture surface generation, fragment morphing, and distortion led to noticeable drops in simulation quality. Fracture surface generation introduced critical variations, while distortion modeling captured clinically relevant misalignments. Morphing fracture areas increased data diversity, further boosting model robustness.

4 Discussion and Conclusion

We present an integrated approach for realistic fracture simulation and robust reduction planning, addressing the challenges of learning fracture-specific features and the scarcity of training data. Our transformer-based network leverages fracture-aware encoding, enabling accurate and generalizable fracture reduction, even in complex cases such as bilateral and sacrum fractures. To generate diverse and realistic synthetic fractures, our approach learns clinical fracture patterns from limited samples. This sim-to-real strategy enables the training of robust models without the need for extensive real fracture datasets. Additionally, by incorporating recursive inference and registration, our method achieves precise alignment and resilience against large displacements.

Extensive experiments demonstrate the superiority of our approach over traditional and learning-based methods, showing significant improvements in planning accuracy. Ablation studies further validate the contributions of individual

components in both the reduction planning framework and the fracture data generation process. Additionally, our method achieved an average runtime of 1.45 seconds, a significant improvement over 42 minutes in the SSM-based method [7].

Since direct statistical modeling of fracture patterns in a latent space is challenging, we instead map clinical fractures onto simulated anatomies and introduce further variations. Preliminary results confirm the robustness and generalizability of this approach, with training on a limited number of fracture modes (38 for the hipbone and 11 for the sacrum) proving sufficient to infer unseen fracture patterns. However, failure cases still occur when fragments lack distinct geometric features, hindering accurate alignment. Future work will explore semantic-aware reconstruction to enhance fragment alignment, and validate the generalizability to irregular fractures and other anatomies.

Acknowledgments. This work was supported by National Natural Science Foundation of China (Grant No. NSFC6247010104), Beijing Science and Technology Project (Grant No. Z221100003522007), and Beijing Jishuitan Research Funding (Grant No. ZR-202504).

Disclosure of Interests. The authors declare that they have no competing interests.

References

1. Adams, J., Elhabian, S.: Point2ssm++: Self-supervised learning of anatomical shape models from point clouds. arXiv preprint arXiv:2405.09707 (2024)
2. Attene, M.: A lightweight approach to repairing digitized polygon meshes. The visual computer **26**, 1393–1406 (2010)
3. Deng, Z., Jiang, J., Chen, Z., Zhang, W., Yao, Q., Song, C., Sun, Y., Yang, Z., Yan, S., Huang, Q., et al.: Tassembly: Data-driven fractured object assembly using a linear template model. Computers & Graphics **113**, 102–112 (2023)
4. Ead, M.S., Palizi, M., Jaremko, J.L., Westover, L., Duke, K.K.: Development and application of the average pelvic shape in virtual pelvic fracture reconstruction. Int J Med Robot **17**(2), e2199 (2021). https://doi.org/10.1002/rcs.2199
5. Ead, M.S., Westover, L., Polege, S., McClelland, S., Jaremko, J.L., Duke, K.K.: Virtual reconstruction of unilateral pelvic fractures by using pelvic symmetry. International Journal of Computer Assisted Radiology and Surgery **15**, 1267–1277 (2020). https://doi.org/10.1007/s11548-020-02140-z
6. Gnat, R., Saulicz, E., Biały, M., Kłaptocz, P.: Does pelvic asymmetry always mean pathology? analysis of mechanical factors leading to the asymmetry. Journal of Human Kinetics **21**(2009), 23–32 (2009). https://doi.org/doi:10.2478/v10078-09-0003-8
7. Han, R., Uneri, A., Vijayan, R.C., Wu, P., Vagdargi, P., Sheth, N., Vogt, S., Kleinszig, G., Osgood, G.M., Siewerdsen, J.H.: Fracture reduction planning and guidance in orthopaedic trauma surgery via multi-body image registration. Med Image Anal **68**, 101917 (2021). https://doi.org/10.1016/j.media.2020.101917
8. Liu, J., Li, H., Zeng, B., Wang, H., Kikinis, R., Joskowicz, L., Chen, X.: An end-to-end geometry-based pipeline for automatic preoperative surgical planning of pelvic fracture reduction and fixation. IEEE Transactions on Medical Imaging (2024). https://doi.org/10.1109/TMI.2024.3429403

9. Liu, P., Han, H., Du, Y., Zhu, H., Li, Y., Gu, F., Xiao, H., Li, J., Zhao, C., Xiao, L., et al.: Deep learning to segment pelvic bones: large-scale ct datasets and baseline models. International Journal of Computer Assisted Radiology and Surgery **16**, 749–756 (2021). https://doi.org/10.1007/s11548-021-02363-8
10. Liu, Y., Yibulayimu, S., Sang, Y., Zhu, G., Wang, Y., Zhao, C., Wu, X.: Pelvic fracture segmentation using a multi-scale distance-weighted neural network. In: International Conference on Medical Image Computing and Computer-Assisted Intervention. pp. 312–321. Springer (2023). https://doi.org/10.1007/978-3-031-43996-4_30
11. Liu, Y., Yibulayimu, S., Sang, Y., Zhu, G., Shi, C., Liang, C., Cao, Q., Zhao, C., Wu, X., Wang, Y.: Preoperative fracture reduction planning for image-guided pelvic trauma surgery: A comprehensive pipeline with learning. Medical Image Analysis p. 103506 (2025). https://doi.org/10.1016/j.media.2025.103506
12. Lu, S., Yang, Y., Li, S., Zhang, L., Shi, B., Zhang, D., Li, B., Hu, Y.: Preoperative virtual reduction planning algorithm of fractured pelvis based on adaptive templates. IEEE Transactions on Biomedical Engineering **70**(10), 2943–2954 (2023). https://doi.org/10.1109/TBME.2023.3272007
13. Luque-Luque, A., Pérez-Cano, F.D., Jiménez-Delgado, J.J.: Complex fracture reduction by exact identification of the fracture zone. Medical Image Analysis **72**, 102120 (2021). https://doi.org/10.1016/j.media.2021.102120
14. Olson, S.A., Furman, B., Guilak, F.: Joint injury and post-traumatic arthritis (2012). https://doi.org/10.1007/s11420-011-9247-7
15. Paulano-Godino, F., Jiménez-Delgado, J.J.: Identification of fracture zones and its application in automatic bone fracture reduction. Computer Methods and Programs in Biomedicine **141**, 93–104 (2017). https://doi.org/10.1016/j.cmpb.2016.12.014
16. Phan, A.V., Le Nguyen, M., Nguyen, Y.L.H., Bui, L.T.: Dgcnn: A convolutional neural network over large-scale labeled graphs. Neural Networks **108**, 533–543 (2018). https://doi.org/10.1016/j.neunet.2018.09.001
17. Sellán, S., Chen, Y.C., Wu, Z., Garg, A., Jacobson, A.: Breaking bad: A dataset for geometric fracture and reassembly. Advances in Neural Information Processing Systems **35**, 38885–38898 (2022)
18. Smith, W., Shurnas, P., Morgan, S., Agudelo, J., Luszko, G., Knox, E.C., Georgopoulos, G.: Clinical outcomes of unstable pelvic fractures in skeletally immature patients. JBJS **87** (2005). https://doi.org/10.2106/JBJS.C.01244v
19. Ulbrich, M., Van den Bosch, V., Bönsch, A., Gruber, L.J., Ooms, M., Melchior, C., Motmaen, I., Wilpert, C., Rashad, A., Kuhlen, T.W., et al.: Advantages of a training course for surgical planning in virtual reality for oral and maxillofacial surgery: crossover study. JMIR Serious Games **11**, e40541 (2023)
20. Willis, A.R., Anderson, D.D., Thomas, T.P., Brown, T.D., Marsh, J.L.: 3d reconstruction of highly fragmented bone fractures. In: SPIE Medical Imaging (2007). https://doi.org/10.1117/12.708683
21. Yibulayimu, S., Liu, Y., Sang, Y., Zhu, G., Wang, Y., Liu, J., Shi, C., Zhao, C., Wu, X.: Pelvic fracture reduction planning based on morphable models and structural constraints. In: International Conference on Medical Image Computing and Computer-Assisted Intervention. pp. 322–332. Springer (2023). https://doi.org/10.1007/978-3-031-43996-4_31
22. Yibulayimu, S., Sang, Y., Liu, Y., Zhu, G., Wang, Y., Zhao, C., Cao, Q., Wu, X.: Automatic pelvic structure restoration: A sim-to-real approach via recursive pose estimation network. In: 2024 IEEE International Symposium on Biomedical Imaging (ISBI). pp. 1–5 (2024). https://doi.org/10.1109/ISBI56570.2024.10635211

23. Yu, X., Rao, Y., Wang, Z., Liu, Z., Lu, J., Zhou, J.: Pointr: Diverse point cloud completion with geometry-aware transformers. In: Proceedings of the IEEE/CVF international conference on computer vision. pp. 12498–12507 (2021)
24. Yu, X., Rao, Y., Wang, Z., Lu, J., Zhou, J.: Adapointr: Diverse point cloud completion with adaptive geometry-aware transformers. IEEE Transactions on Pattern Analysis and Machine Intelligence **45**(12), 14114–14130 (2023). https://doi.org/10.1109/TPAMI.2023.3309253
25. Zeng, B., Wang, H., Tao, X., Shi, H., Joskowicz, L., Chen, X.: A bidirectional framework for fracture simulation and deformation-based restoration prediction in pelvic fracture surgical planning. Medical Image Analysis **97**, 103267 (2024). https://doi.org/10.1016/j.media.2024.103267
26. Zhang, L.h., Zhao, J.x., Zhao, Z., Su, X.y., Zhang, L.c., Zhao, Y.p., Tang, P.f.: Computer-aided pelvic reduction frame for anatomical closed reduction of unstable pelvic fractures. Journal of Orthopaedic Research **34**(1), 81–87 (2016). https://doi.org/10.1002/jor.22987
27. Zhao, C., Cao, Q., Sun, X., Wu, X., Zhu, G., Wang, Y.: Intelligent robot-assisted minimally invasive reduction system for reduction of unstable pelvic fractures. Injury **54**(2), 604–614 (2023). https://doi.org/10.1016/j.injury.2022.11.001
28. Zhao, C., Guan, M., Shi, C., Zhu, G., Gao, X., Zhao, X., Wang, Y., Wu, X.: Automatic reduction planning of pelvic fracture based on symmetry. Computer Methods in Biomechanics and Biomedical Engineering: Imaging & Visualization **10**(6), 577–584 (2022). https://doi.org/10.1080/21681163.2021.2012830